Surfaces and Interfaces 55 (2024) 105413

Contents lists available at ScienceDirect

Surfaces and Interfaces

journal homepage: www.sciencedirect.com/journal/surfaces-and-interfaces

Stacking order and vertical strain controllable optoelectronic properties of van der Waals heterostructures constructed with germanene and double layer hexagonal structure AlAs

Gang Guo [a,*], Yongcheng Chen [a], Lingyun Mao [a], Ping Li [b,*]

[a] School of Science, Hunan Institute of Technology, Hengyang 421002, China
[b] State Key Laboratory for Mechanical Behavior of Materials, Center for Spintronics and Quantum System, School of Materials Science and Engineering, Xi'an Jiaotong University, Xi'an 710049, China

ARTICLE INFO

Keywords:
DLHS-AlAs monolayer
Germanene monolayer
Van der Waals heterostructures
Optoelectronic properties
First-principles calculations

ABSTRACTS

In this study, we use first-principles calculations to investigate the structural and optoelectronic properties of DLHS-AlAs/germanene van der Waals heterostructures (vdWHs) with different stacking orders and vertical strain. The AIMD calculations and binding energies demonstrate that all three DLHS-AlAs/germanene vdWHs are thermally and energetically stable. The interesting transitions from semiconductor to metal and type-I to type-II band alignment can be observed in AB stacking vdWH under vertical strain regulation. Meanwhile, the Dirac cone is always well preserved in all vdWHs. The calculated optical absorption spectra indicate that all vdWHs show enhanced light absorption across the ultraviolet to visible light range, compared to their individual components. Besides, the application of vertical strain can result in the weakening or enhancement of ultraviolet light absorption coefficients in different regions of all vdWHs. Of particular interest is the observation that optical adsorption in the visible light region for all vdWHs is almost always enhanced and broadened with increasing vertical compression strain. These excellent and tunable optoelectronic properties suggest that DLHS-AlAs/germanene vdWHs may have favourable potential for use in optoelectronic devices.

Introduction

In light of the considerable success of two-dimensional (2D) graphene in experimental research [1-2], theoretical studies and practical applications [3-7], the group-IV monolayers including silicene [8], germanene [9] and other layered materials [10], have also garnered significant interest due to their exceptional physical properties and potential for application in electronic devices. In 2014, the synthesis of germanene, a material comprising a single germanium atomic layer and a buckled hexagonal lattice, was achieved on the surface of Pt by ultra-high vacuum physical vapor deposition [11]. Subsequently, researchers have continued to report the preparation of germanene on surfaces of aluminium, silver and gold [12-14]. In contrast to graphene, germanene exhibits a distinctive buckled structure, which endows it with a range of exceptional properties, including remarkable tensile resistance [15], a high spin-orbit coupling effect [16] and a quantum spin Hall effect [17]. Moreover, in recent years, research on germanene has been conducted in a number of different fields, including gas sensing [18], electrode materials [19] and even theranostic materials [20]. In particular, germanene, like graphene, has a high carrier mobility [21], which makes it an ideal material for integration in germanium-based electronics. This makes it a promising transistor material for a new generation of semiconductor devices.

However, the feature of a tiny band gap of germanene severely restricts its further applications in electronic and optoelectronic devices. For example, a transistor channel material must possess a band gap exceeding 0.1eV [22]. Besides, good photoelectric materials must have proper optical property such as high light absorption [23]. It may therefore be posited that modifying the optoelectronic properties of germanene may prove an efficacious method of enabling it to serve as an excellent candidate material in the field of semiconductor optoelectronic devices. Conventional methods for modifying the physical properties of two-dimensional materials include strain engineering [24-25], doping [26-27] and external electric field [28-29], and other techniques. While the aforementioned methods can enhance certain physical properties and even induce new ones, in most cases, this is achieved at the

---

* Corresponding author.
E-mail addresses: ggxhsg@126.com (G. Guo), pli@xjtu.edu.cn (P. Li).

https://doi.org/10.1016/j.surfin.2024.105413
Received 3 August 2024; Received in revised form 25 October 2024; Accepted 7 November 2024
Available online 8 November 2024

expense of some of germanene's intrinsic properties, such as the destruction of the Dirac cone and a reduction in carrier mobility. This highlights the need for a more optimal approach that not only tunes the excellent properties but also retains the high carrier mobility characteristic of germanene.

Recently, surface science, which focuses on solid/vacuum, solid/gas, and solid/solid interfaces [30], has emerged as a research hotspot in the fields of materials science and nanotechnology. Particularly, heterostructure engineering, as an important research direction of surface science, offers a viable solution for the precise control and design of solid/solid nanoscale surface structures, thereby advancing the development of surface science and technology. Through heterostructure engineering, the physical properties of two-dimensional materials can be effectively regulated [31-32]. Generally, the formation of a heterostructure can lead to enhanced performance and the emergence of novel properties, provided that the intrinsic characteristics of the constituent materials are maintained. For example, a DFT study [33] reported that the GeSe/SnSe van der Waals heterostructure (vdWH) exhibited higher visible light absorption than its individual constituents, making it a promising candidate for solar cells. Meanwhile, the sensing capabilities of GeSe and SnS monolayers can be enhanced through the construction of GeSe/SnS vdWHs [34]. Similarly, signatures of moiré-trapped valley excitons have been observed in $MoSe_2/WSe_2$ [35] and WSe_2/WS_2 [36] vdWHs. Furthermore, several studies have examined the physical properties of heterostructures composed of semiconductors and group-IV 2D materials. For instance, Luo et al. [37] demonstrated that both enhanced light absorption in the visible spectrum and Ohmic contact can be achieved in HfSeX (X = S or Se)/graphene vdWHs. A MoS_2/graphene vdWH [38] has been shown to exhibit a high degree of sensitivity to light, making it an excellent candidate for use in graphene-based photodetectors. Mishchenko et al. [39] also indicated that a WS_2/graphene vdWH can be designed to function as an ideal vertical field-effect transistor due to its high ON current at room temperature. It is important to note that graphene-based vdWHs exhibit several other noteworthy properties, including electronic transport [40], gas detection [41], the quantum anomalous Hall effect [42], and charge and spin transport [43]. Meanwhile, vdWHs based on antimonene have also garnered significant attention. The antimonene/WS_2 vdWHs [44] have demonstrated both high photoelectric power conversion efficiency and type-II band alignment. A first-principles study indicated that the antimonene/bismuthene vdWH [45] has potential applications in beam splitters and nanoscale mirrors due to its high structural stability and favorable photoelectric properties.

With regard to germanene, the initial consideration may be to construct heterostructures with germanene and metallic substrates, given the successful preparation of germanene on metal surfaces. Although germanene/metal heterostructure can exhibit good structural stability, the strong interaction between germanene and metallic substrate can lead to the destruction of the Dirac cone, which will cause a decrease in carrier mobility. Therefore, identifying suitable substrates for the construction of heterostructures with germanene represents a promising avenue for further research. In a recent study, Sengupta et al. [46] have predicted the excellent photo-absorption properties of InSe/germanene vdWH. Additionally, Pang et al. [47] have reported that germanene/MoS_2 vdWH can exhibit controllable electronic and optical properties under strain, rendering it suitable for use in the field of optoelectronic devices. Similarly, extensive research has been conducted on the electronic and optical properties of germanene-based vdWHs, including monolayer CdS/germanene [48], germanene/2D-SiC [49], and germanene/ZnSe [50]. These significant studies clearly demonstrate that various combinations of interfaces result in distinct properties, greatly enhancing their applications.

A recently discovered 2D hexagonal lattice semiconductor, constructed with aluminium and arsenic elements, has attracted the attention of researchers due to its distinctive structure and properties [51]. This monolayer AlAs exhibits a double layer hexagonal structure (DLHS), which differs from the single layer hexagonal structure. Bafekry et al. [51] have additionally postulated that the DLHS AlAs monolayer exhibits robust structural stability and noteworthy optical and electronic properties. Furthermore, analogous DLHS 2D monolayers, such as AlSb [52] and InSb [53], have been successfully synthesised in experiments. This evidence suggests that the preparation of a DLHS AlAs monolayer may be achievable in the future through the molecular beam epitaxy method. Meanwhile, the lattice constants of DLHS AlAs monolayer and germanene are so close that they form heterostructure with a nearly zero lattice mismatch, which is very beneficial to the experimental preparation of the heterostructure. So, the DLHS AlAs monolayer may be a proper component material for germanene-based vdWH.

Herein, our paper employs first-principles calculations based on density functional theory (DFT) to study the structural stability and optoelectronic properties of DLHS-AlAs/germanene vdWHs under diverse stacking orders and vertical strain conditions. The calculated findings indicated that the vdWHs can possess good stability, controllable and enhanced optoelectronic properties, including type-I or type-II band alignment, direct band gap, and high light absorption in the visible light region. It is our hope that this investigation will provide a solution for modulating the properties of germanene-based materials and broadening their application in the field of optoelectronic devices.

2. Computational Methods

The Vienna ab initio simulation package (VASP) based on density functional theory (DFT) [54] was employed to carry out the calculations. The projector-augmented wave (PAW) pseudopotentials and the exchange-correlation function including the generalized gradient approximation (GGA) as well as the Perdew-Burke-Ernzerhof (PBE) function [55-57] were also used in the calculations. To obtain accurate results, the hybrid functional of Heyd-Scuseria-Ernzerhof (HSE06) [58] was considered to calculate the electronic properties. The cut-off energy of 550 eV and a Monkhorst-Pack k-point grid of 11 × 11 × 1 were used for the structural optimization. A lager k-point grid of 33 × 33 × 1 was used to calculate the electronic and optical properties. The force on each atom and the convergence criteria in energy were set at 0.01 eV/Å and 10^{-5} eV, respectively. A vacuum thickness more than 15 Å was used to avoid any interactions between adjacent cells. To consider the van der Waals interaction of the vdWH, the DFT-D3 method [59] was used in calculations. In addition, the PHONOPY package [60] was used to perform the calculation of the phonon spectrum. And the ab initio molecular dynamics (AIMD) simulation was also used to to evaluate the thermal stability at 300 K for 6 ps based on a 4 × 4 × 1 supercell.

The charge density difference (CDD) is calculated by the following formula:

$$\Delta\rho = \rho_{\mathrm{H}} - \rho_{AlAs} - \rho_{G} \tag{1}$$

where $\Delta\rho$ is the charge density difference of the system. The ρ_H, ρ_{AlAs} and ρ_G are the total charge densities of the heterostructure, DLHS-AlAs monolayer and germanene, respectively.

The optical absorption coefficient $\alpha(\omega)$ is calculated by the following formula

$$\alpha(\omega) = \sqrt{2}\omega\left[\sqrt{\varepsilon_1^2(\omega) + \varepsilon_2^2(\omega)} - \varepsilon_1(\omega)\right]^{1/2} \tag{2}$$

where the real part and imaginary part of the complex dielectric function are represented by $\varepsilon_1(\omega)$ and $\varepsilon_2(\omega)$, respectively.

3. Results and Discussion

3.1. The study of pristine germanene and DLHS-AlAs monolayers

The accuracy of subsequent calculations of heterojunctions is first ensured by investigating the pristine germanene and DLHS-AlAs monolayers. As illustrated in Fig. 1(a), the relaxed germanene monolayer exhibits a buckled hexagonal lattice with a lattice constant of 4.056 Å (see Table 1), which is in good agreement with the findings of a previous study [61]. The calculated phonon spectrum exhibits no imaginary frequencies, thereby indicating the dynamically stable nature of the germanene monolayer. It is also observed that germanene exhibits semimetal characteristics when calculated using the PBE method. In contrast, the band structure calculated using the HSE06 method shows a narrow band gap of 0.10 eV, which is also similar to that reported by Hoat et al. [61]. As illustrated in Fig. 1(b), the monolayer AlAs exhibits a double-layer hexagonal structure, which differs from the AlAs monolayer with a single-layer hexagonal structure [62]. The lengths of the Al-As bonds in the plane and vertically are 2.475 Å and 2.649 Å, respectively. Furthermore, the relaxed lattice constant is 4.021 Å (see Table 1), which is consistent with the previously reported value of 3.99 Å [51]. The DLHS-AlAs monolayer also exhibits excellent stability, as evidenced by the absence of imaginary frequencies. Furthermore, the PBE method indicates a band gap of 1.21 eV for the DLHS-AlAs monolayer, while the HSE06 method yields a wider band gap of 1.84 eV. Given that the PBE method tends to underestimate the band gap of semiconductors, the latter result is deemed to be reasonable. Consequently, the HSE06 method will be employed in the subsequent calculations of band gaps.

3.2. *The study of germanene/DLHS-AlAs vdWHs with different stacking orders*

It is widely acknowledged that the lattice mismatch represents a fundamental consideration in the design of a heterostructure. The calculated results demonstrate that the lattice constants of germanene and DLHS-AlAs are 4.056 Å and 4.021 Å, respectively. Thus, the unit cell of heterostructure can be composed by the primitive cells of germanene and DLHS-AlAs. In this study, we present three different stacking heterostructures (AA, AB and AC), as illustrated in Fig. 2. As indicated in Table 1, the lattice constants of the aforementioned structures are 4.031 Å, 4.033 Å and 4.030 Å, respectively. Furthermore, the height between germanene and DLHS-AlAs in the direction of the vacuum layer is 3.291 Å (AA), 3.084 Å (AB) and 3.358 Å (AC), respectively. Additionally, the lengths of the Al-As and Ge-Ge bonds in vdWHs are nearly identical to those of the corresponding component materials. Notably, the calculated lattice mismatch is approximately 0.9 %, which is relatively minor and acceptable. To confirm the stability of the vdWHs, the binding energy is calculated by the following formula:

$$E_b = E_H - E_1 - E_2 \tag{3}$$

In this formula, E_H is the total energy of heterostructure; E_1 and E_2 represent the the total energies of individual components. As defined, a more negative binding energy means a more stable system. As listed in Table 1, the values of binding energy per cell for AA, AB and AC vdWHs are -0.244 eV, -0.302 eV and -0.204 eV, respectively. In the three van der Waals heterostructures, the distances of the Ge-Ge and Al-As bonds exhibit minimal variation in comparison to those observed in the individual components. This suggests that all three vdWHs are capable of maintaining a stable geometric structure. To further confirm their stability, ab initio molecular dynamics (AIMD) simulations were performed. As illustrated in Fig. 3, it is evident that during thermal vibration, the energy of each atom in all systems exhibits fluctuations within the range of 0.05 eV. Moreover, following a 6 ps heating period at 300K, the structural integrity of each heterostructure is observed to remain intact, indicating a high degree of stability for these heterostructures.

Fig. 4 presents the projected band structures and corresponding partial density of states (PDOS) of the AA, AB and AC vdWHs, as calculated using the HSE06 method. The contributions of the germanene and double layer hexagonal structure AlAs to the projected bands of the vdWHs are indicated by blue and red circles, respectively. The band structures indicate that all the vdWHs exhibit direct bandgap semiconducting behaviour, with the CBM and VBM originating from the π and π* states of germanene, respectively, suggesting a type-I band arrangement. Furthermore, the breaking of germanene symmetry in these heterojunctions has resulted in the opening of significant band gaps in the AA (191 meV), AB (234 meV) and AC (171 meV) vdWHs, exceeding those observed in the germanene/MoS_2 vdWH (62 meV) and in pristine monolayer germanene (101 meV). It is evident that the Dirac cone is well preserved in each vdWH, indicating that high carrier mobility can be maintained in these heterojunctions. The PDOS curves for each heterojunction demonstrate that the CBM and VBM originate from the p_z orbital of Ge, confirming a semiconducting character, which

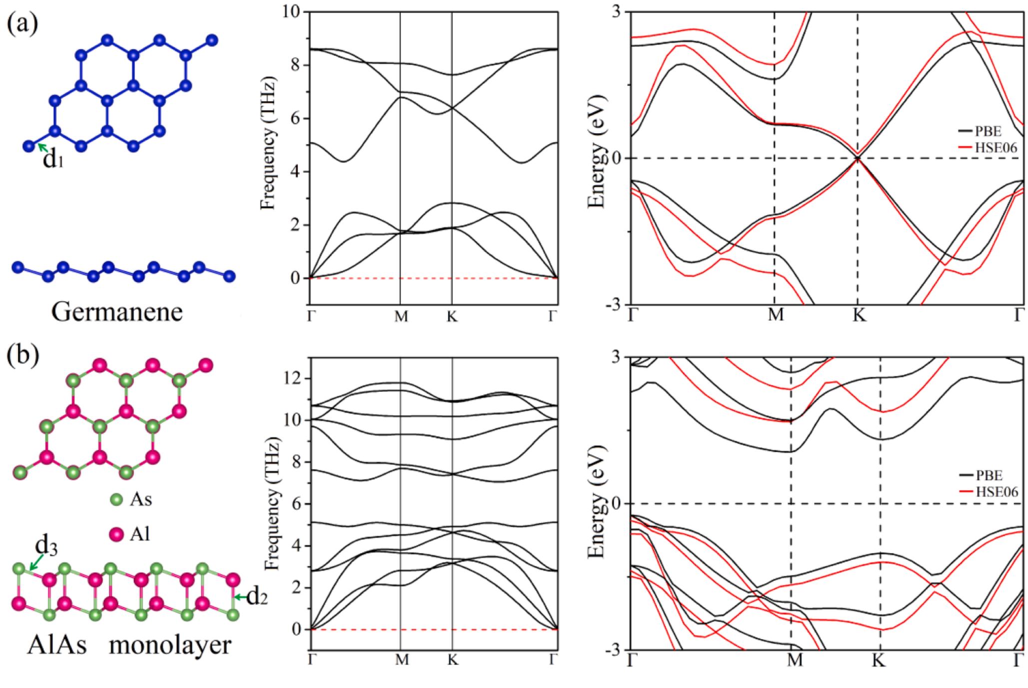

Fig. 1. The optimized structures, phonon dispersion curves and band structures for germanene and DLHS-AlAs monolayers.

Table 1

Summary of the calculated results of Germanene/DLHS-AlAs vdWHs and corresponding monolayers. a (Å) is the lattice constant. E_b is the binding energy. D (Å) is the bond length and h (Å) is the the interlayer distance for vdWH. The band gaps of germanene (Δ_1) and vdWH (Δ_2) are indicated, where the band gap calculated by HSE06 method is indicted in brackets.

Systems	a (Å)	E_b (eV)	D (Å)			h (Å)	Δ (meV)	
			d_1	d_2	d_3		Δ_1	Δ_2
Germanene	4.056	/	2.442	/	/	/	/	/
AlAs monolayer	4.021	/	/	2.649	2.475	/	/	/
AA vdWH	4.031	-0.244	2.433	2.652	2.478	3.291	85 (191)	85 (191)
AB vdWH	4.033	-0.302	2.446	2.653	2.481	3.084	121 (234)	121 (234)
AC vdWH	4.030	-0.224	2.433	2.649	2.478	3.358	103 (171)	103 (171)

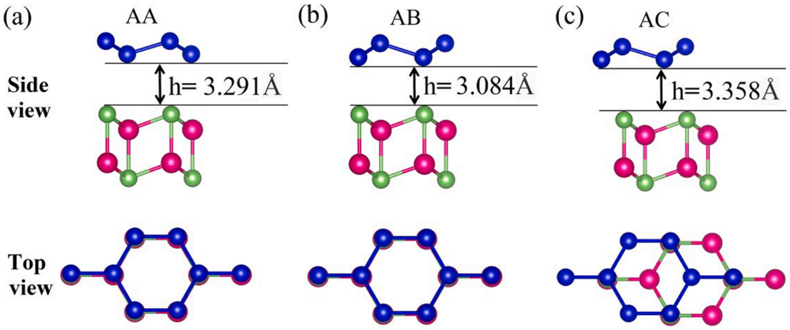

Fig. 2. The optimized structures of top and side views for AA, AB and AC vdWHs.

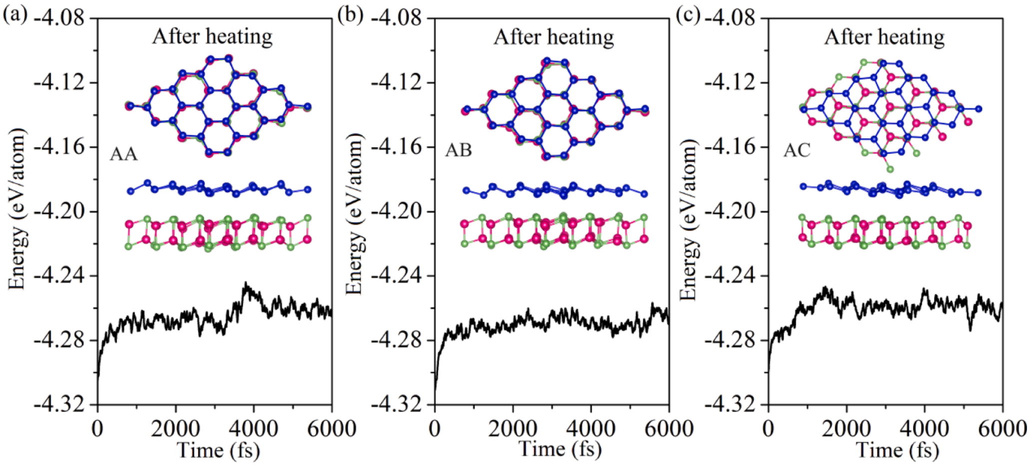

Fig. 3. The energy fluctuations for AA, AB and AC vdWHs during the Ab initio molecular dynamic (AIMD) simulations at 300 K.

is consistent with the band structure analysis.

In order to study the optical features of AA, AB and AC vdWHs, the optical absorption coefficients in the vertical plane direction are calculated in Fig. 5. As illustrated in Fig. 5(a), in the ultraviolet region, the maximum value of optical absorption coefficients for DLHS-AlAs/germanene vdWHs is approximately 18 × 10^5 cm^{-1}, which is considerably higher than that of germanene and only moderately lower than that of DLHS-AlAs. Similarly, as illustrated in Fig. 5(b), in the visible light region, the maximum value of optical absorption coefficients for AA, AB and AC vdWHs can reach 3.4 × 10^5 cm^{-1}, 6.5 × 10^5 cm^{-1} and 2.3 × 10^5 cm^{-1}, respectively, which are significantly larger than those of individual DLHS-AlAs and germanene monolayers. Furthermore, in comparison to the visible light absorption capacity of other two-dimensional vdWHs, such as Ga_2SeTe/In_2SSe (0.6 × 10^5 cm^{-1}) [63] and $WSeTe/C_3N_4$ (2 × 10^5 cm^{-1}) [64], the DLHS-AlAs/germanene vdWH with AB stacking exhibits significantly enhanced optical absorption, indicating its potential for favourable application in photoelectric devices.

3.3. *Vertical strain effects on the DLHS-AlAs/germanene vdWHs*

Previous studies have indicated that the vertical strain can modify the electronic properties of vdWHs [65-66]. Thus, we also investigate the vertical strain effects on optoelectronic properties of DLHS-AlAs/germanene vdWHs. Herein, the vertical compressive strain coefficient (ε) is considered, which can be calculated as $\varepsilon = (l_0 - l)/l_0 \times 100\%$, in which l and l_0 mean the interlayer distance for strained and unstrained heterostuctures. We first use the strain energy to examine the stability of strained DLHS-AlAs/germanene vdWHs. As listed in Table 2, as the strain increases from 0% to 10%, the strain energy of all heterostuctures show a linear increase. However, the range of this strain energy change is small, less than 0.05eV, which means that the strained heterostuctures can preserve a reasonable geometric structure.

Next, the electronic band structures of DLHS-AlAs/germanene vdWHs under 2%, 6% and 10% vertical compressive strains, as calculated by the HSE06 method, are subsequently examined. As illustrated in Fig. 6(a), the AA vdWH exhibits a direct semiconductor behaviour under

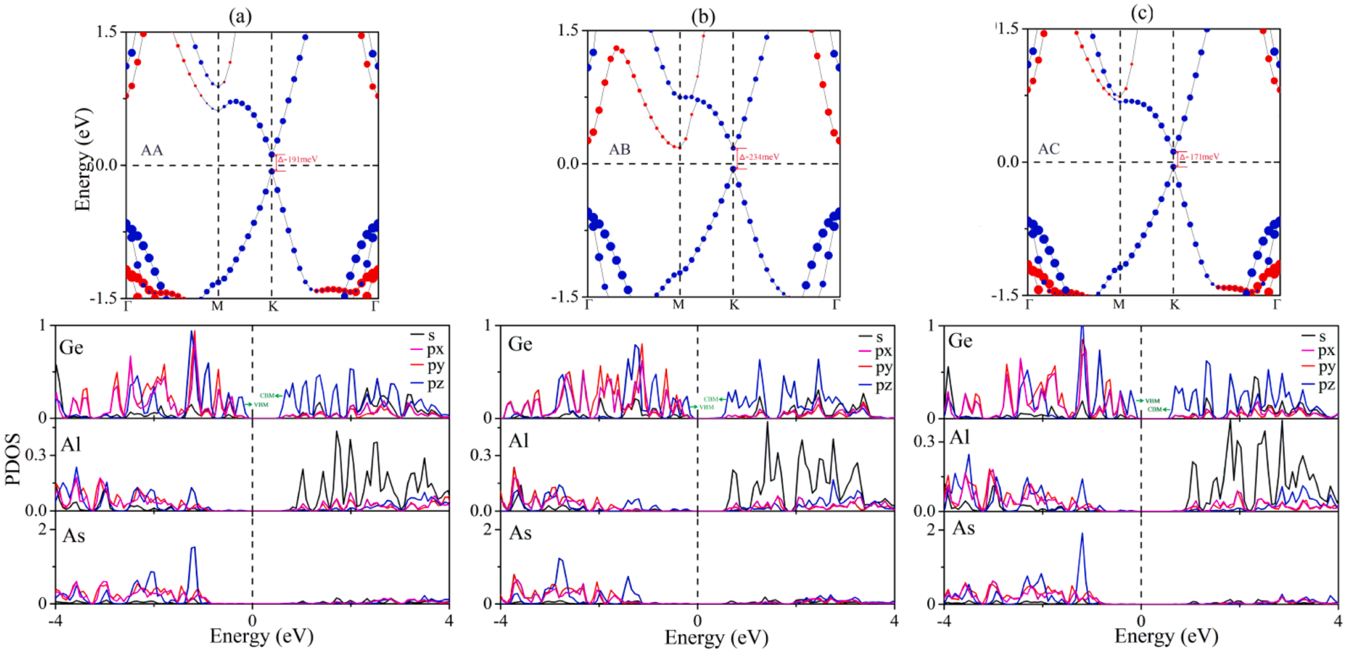

Fig. 4. The projected band structures and corresponding partial density of states (PDOS) for AA, AB and AC vdWHs as calculated by HSE06 method.

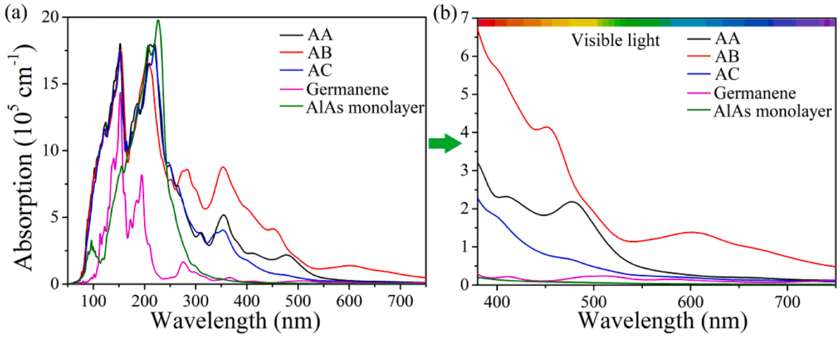

Fig. 5. The optical absorption coefficients of AA, AB and AC vdWHs as well as individual monolayers.

Table 2
Summary of the calculated results of Germanene/DLHS-AlAs vdWHs under vertical strain. E_s is the strain energy. The band gaps of germanene (Δ_1) and vdWHs (Δ_2) are indicated, where the band gap calculated by HSE06 method is indicted in brackets.

Systems	Strain (%)	E_s (eV)	Δ_1 (meV)	Δ_2 (meV)
AA vdWH	2	0.0022	96 (205)	96 (205)
	4	0.0066	107 (224)	107 (224)
	6	0.0135	120 (239)	120 (239)
	8	0.0231	133 (259)	133 (259)
	10	0.0356	148 (293)	148 (293)
AB vdWH	2	0.0024	154 (412)	157 (307)
	4	0.0083	185 (296)	92 (181)
	6	0.0171	217 (329)	72 (153)
	8	0.0293	240 (372)	60 (123)
	10	0.0468	280 (401)	41 (94)
AC vdWH	2	0.0027	118 (187)	118 (187)
	4	0.0072	135 (208)	135 (208)
	6	0.0144	154 (230)	154 (230)
	8	0.0244	174 (259)	174 (259)
	10	0.0375	197 (294)	197 (294)

diverse strains. Moreover, the Dirac cone remains intact, and the Dirac gap can be augmented with an increase in strain. As illustrated in Table 2, the Dirac gap of the AA vdWH exhibits a notable increase from 205 meV to 293 meV as the strain magnitude rises from 2% to 10%. Similarly, as illustrated in Fig. 6(c), the same trend is observed in the AC vdWH. The direct band gap (Dirac gap) increases from 187 meV to 294 meV with the strain increasing from 2% to 10%. In contrast, the AB vdWH exhibits a Dirac gap that is consistently larger than that of the AA or AC vdWH, as illustrated in Fig. 6(b). In particular, the Dirac gap can reach 412 meV under 2% strain. As demonstrated in Table 2, the Dirac gap exhibits a notable increase from 296 meV to 401 meV when the applied strains range from 4% to 10%. It is also noteworthy that, under strain, the CBM and VBM of the AB vdWH are situated at disparate points within the Brillouin zone, resulting in an indirect semiconductor character that differs from the direct semiconductor character observed in unstrained AB vdWH. Furthermore, it can be observed that the CBM and VBM of germanene consistently exceed those of DLHS-AlAs, indicating a type-II band alignment. In addition, it can be observed that the CBM of DLHS-AlAs shifts downward with increasing strain, indicating that the band gap of AB vdWH may decrease with increasing strain. Notably, as illustrated in Fig. 7(a), the band gap of AB vdWH decreases from 307 meV to 38 meV with increasing strain from 2% to 14%. A notable transition from the semiconductor to the metallic phase occurs at a strain of 16%. To further substantiate this assertion, the band structure of AB vdWh under 16% strain is discussed in Fig. 7(b). It is evident that a band derived from DLHS-AlAs intersects the Fermi level, indicating a metallic character that is analogous to that observed in the

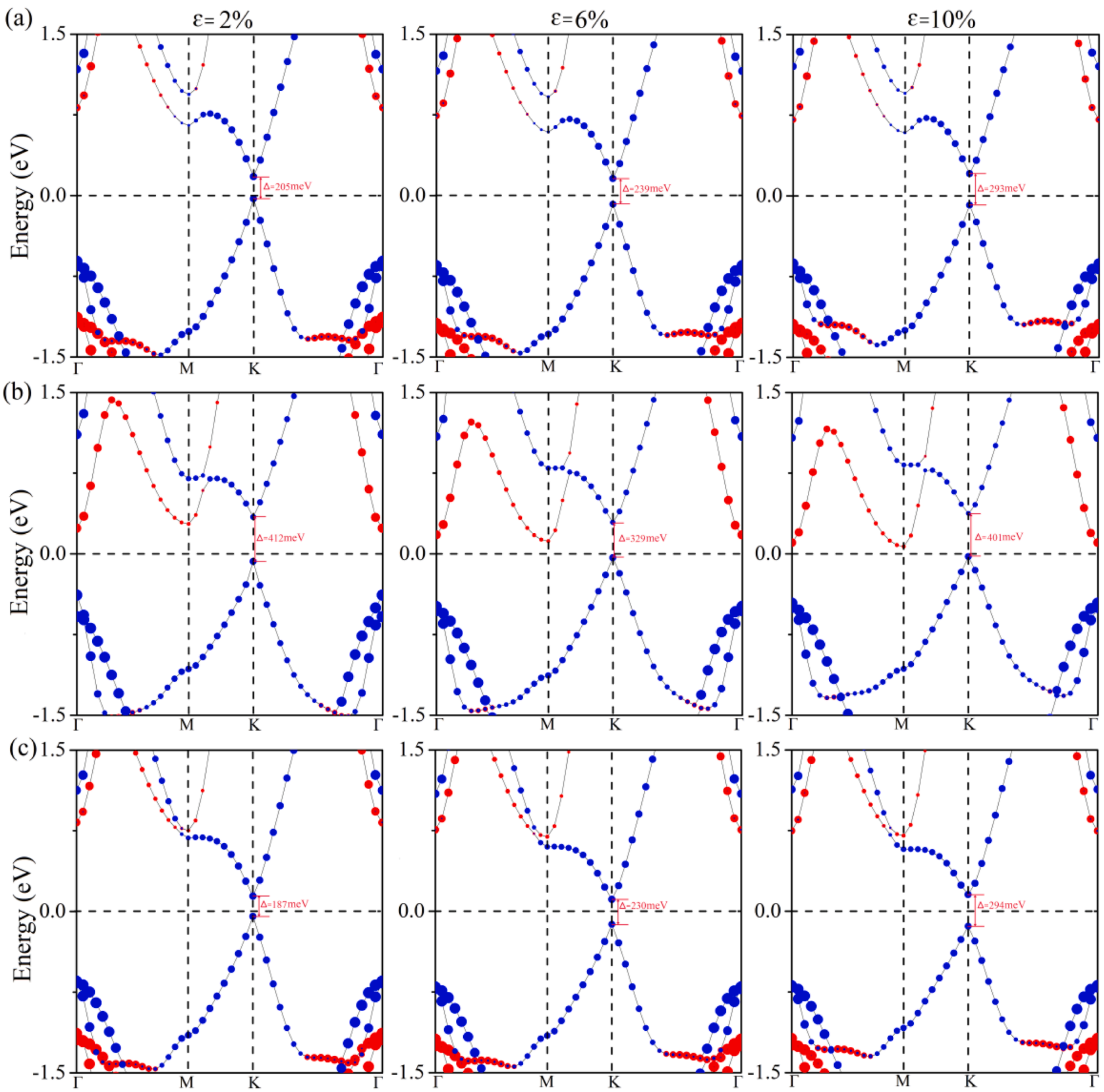

Fig. 6. The projected band structures of AA, AB and AC vdWHs under 2%, 6% and 10% vertical compressive strains.

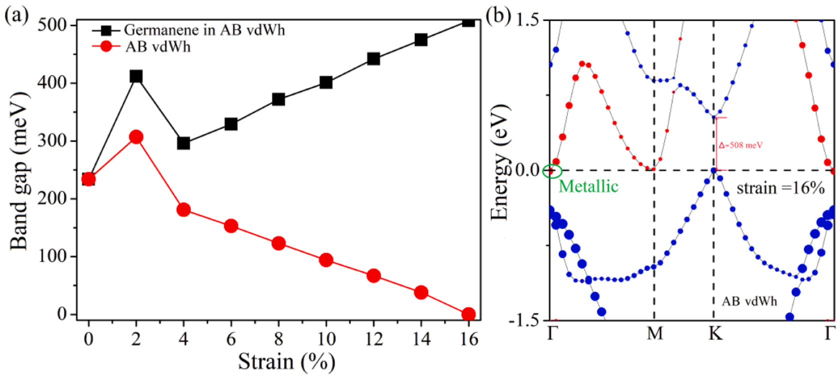

Fig. 7. (a) The Dirac gap of germanene and the band gap of AB vdWH as a function of the strain. (b) Projected band structures of AB vdWH under 16% vertical compressive strain.

MoSSe/germanene heterostructure subjected to 8% tensile strain [67]. In conclusion, the above analysis demonstrates that the Dirac cone of germanene can be preserved in all vdWHs under the strains discussed, which suggests that the highly intrinsic carrier mobility of germanene can be maintained in DLHS-AlAs/germanene vdWHs. Furthermore, the band gap of the DLHS-AlAs/germanene van der Waals heterostructure can be effectively tuned by vertical compressive strain, thereby broadening the potential applications of germanene-based heterostructures in electronic devices.

In order to investigate the impact of vertical compressive strain on vdW interactions in DLHS-AlAs/germanene heterostructures, the planar-averaged charge density difference (CDD) along the z-direction and the amount of charge transfer obtained from Bader charge analysis of the heterostructures are presented in Fig. 8. As illustrated in Figs. 8 (a)-(c), it is evident that electrons predominantly accumulate near DLHS-AlAs (yellow area) and are depleted near germanene (blue area). Given that the work function of DLHS-AlAs is greater than that of germanene, the formation of the heterostructure results in the migration of electrons from germanene to DLHS-AlAs. This phenomenon is analogous to that observed in HfSeX (X=S, Se)/graphene vdWHs [37]. Consequently, germanene functions as a donor, losing electrons, while the DLHS-AlAs monolayer acts as an acceptor, gaining electrons. It is observed that the amount of charge transfer from germane to DLHS-AlAs in each cell gradually increases with the increase of compressive strain. In particular, as illustrated in Fig. 8(d), for the AA vdWH, the amount of charge transfer per cell exhibits a gradual increase from 0.018 e to 0.023 e with the strain rising from 0% to 10%. Similarly, as illustrated in Figs 8 (e) and (f), the same trend is also observed in AB (0.009 e to 0.026 e) and AC vdWHs (0.017 e to 0.024 e). The reason for this increasing charge transfer is that with the increase of vertical compression strain, the layer spacing of the heterojunction decreases gradually, which leads to the strengthening of interlayer interaction. Consequently, stronger interlayer interaction results in a greater charge transfer at the vdWHs interface. These analyses demonstrate that the charge transfer from germanene to DLHS-AlAs is tunable, indicating that the magnitude of the built-in electric field can also be regulated by vertical compression strain.

The optical absorption coefficients in the vertical plane direction of all vdWHs are discussed in Fig. 9. As illustrated in Fig. 9(a), for the AA vdWH case, the optical adsorption in the ultraviolet light region (0-220 nm) exhibits a slight decrease as the vertical compression strain increases gradually. The maximum optical adsorption coefficient remains at 18 × 10^5 cm^{-1}. However, there is a notable enhancement in the optical adsorption coefficients in the ultraviolet light region (250-380 nm) and the visible light region (380-760 nm). It is evident that as the strain increases, the light absorption coefficient rises in a gradual manner. Notably, under a vertical strain of 10%, the maximum optical adsorption coefficient can reach 4.4 × 10^5 cm^{-1}, which is significantly higher than that of untrained AA vdWH (3.4 × 10^5 cm^{-1}). As illustrated in Fig. 9(b), the optical adsorption in the ultraviolet light region (0-200 nm) also exhibits a slight decline with the increase in vertical compression strain for AB vdWH. It can be found that the optical adsorption in the ultraviolet light region (210-340 nm) is markedly enhanced. In the visible light region, the maximum optical adsorption coefficient under strain can still be maintained at a high value of 6.5 × 10^5 cm^{-1}, which is comparable to that of untrained AB vdWH. It is also noteworthy that in the majority of visible regions (410-580 nm and 650-760 nm), the optical adsorption consistently increases with the rise in vertical compression strain. The greatest increase observed was approximately 2.0 × 10^5 cm^{-1}. In the case of AC vdWH, as illustrated in Fig. 9(c), the optical adsorption in the ultraviolet light region (0-230 nm) is also observed to decrease slightly with increasing vertical compression strain. Conversely, the optical adsorption in the ultraviolet light region (230-380 nm) and the visible light region (380-760 nm) is observed to gradually increase. In the visible light region, the maximum optical adsorption coefficients under strain exhibit the following trends: 10% (3.81 × 10^5 cm^{-1}) > 8% (3.15 × 10^5 cm^{-1}) > 6% (2.83 × 10^5 cm^{-1}) > 4% (2.62 × 10^5 cm^{-1}) > 2% (2.48 × 10^5 cm^{-1}) > 0% (2.30 × 10^5 cm^{-1}). Overall, the applied vertical compression strains have been demonstrated to effectively tune the optical adsorption of DLHS-AlAs/germanene vdWHs. In particular, the optical adsorption in the visible light region has been shown to be enhanced and broadened, which suggests that these materials have excellent potential for use in optical devices.

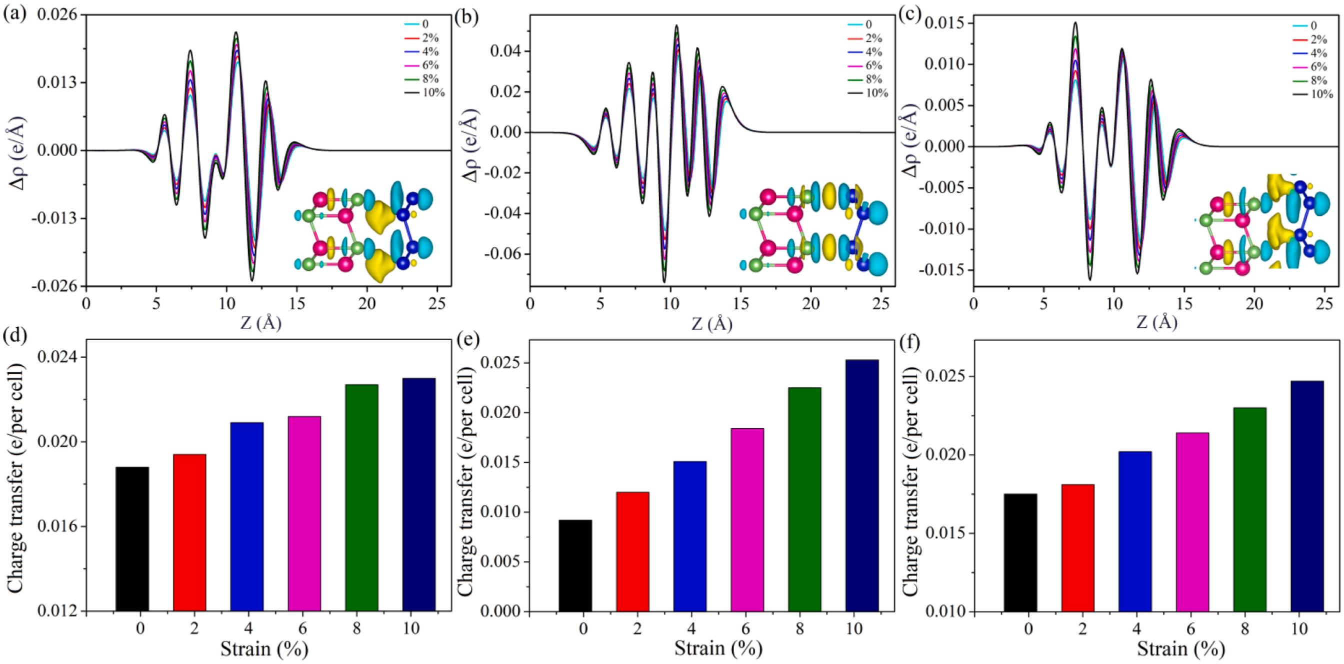

Fig. 8. The the planar-averaged charge density difference (CDD) along the z-direction and the amount of charge transfer of AA, AB and AC vdWHs under vertical compressive strains. (a) and (d) AA vdWH, (b) and (e) AB vdWH, (c) and (f) AC vdWH.

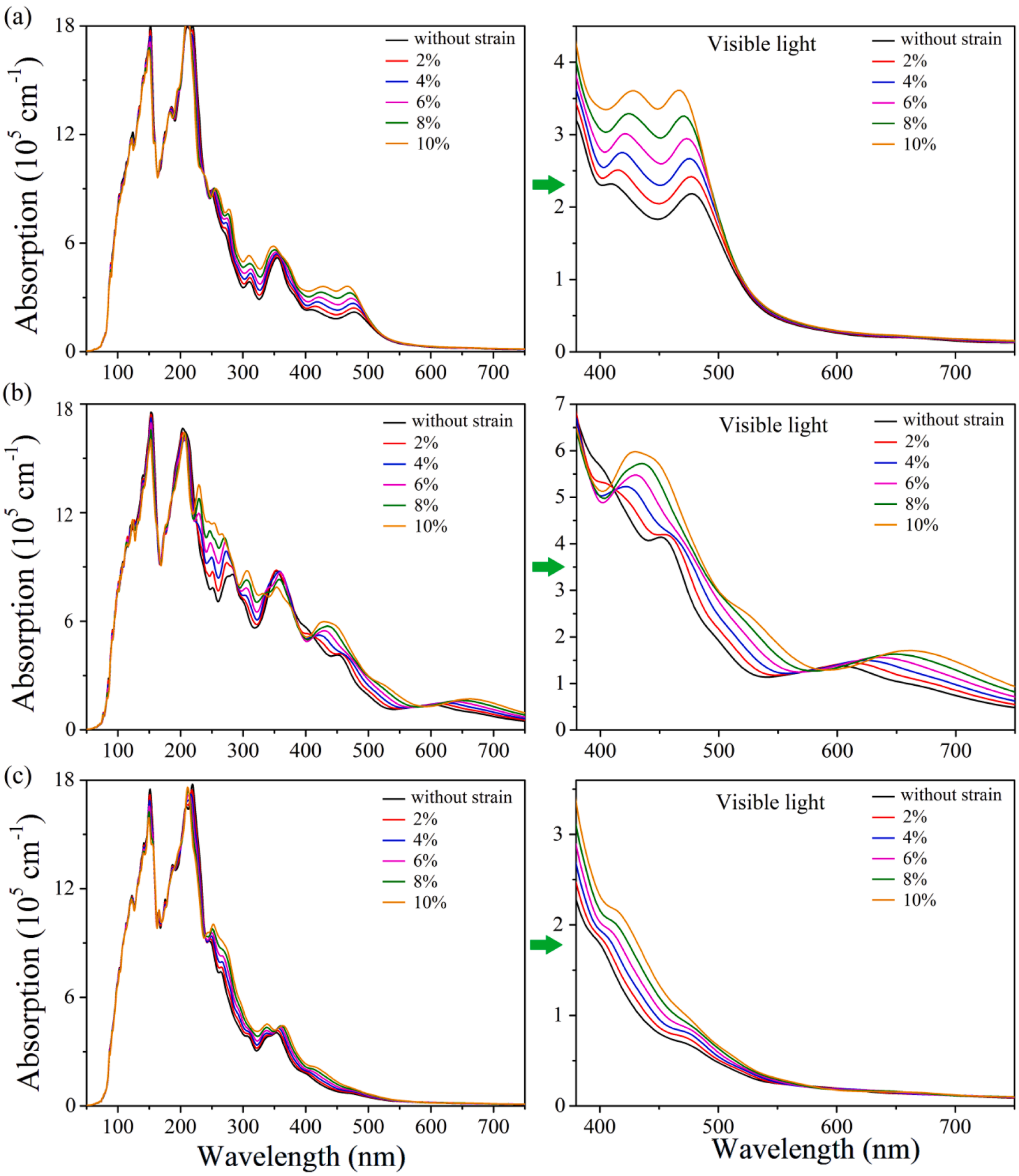

Fig. 9. The optical absorption coefficients of AA, AB and AC vdWHs under vertical compressive strains.

4. Conclusions

In this work, through first-principles calculations, the structural, electronic, and optical properties of DLHS-AlAs/germanene vdWHs with different stacking orders and vertical strain are comprehensively discussed. The results of the phonon spectra analysis demonstrate the stability of the individual DLHS-AlAs and germanene monolayers. It is found that all three DLHS-AlAs/germanene vdWHs exhibit excellent stability. Additionally, all vdWHs display direct semiconductor characteristics and a type-I band alignment. Moreover, the Dirac cone of germanene is well preserved in all vdWHs. As the vertical compression strain is increased, the Dirac gap of AA and AB vdWHs can be made to continuously increase. Nevertheless, the band alignment of the AB stacking vdWH can undergo a transition from type-I to type-II under the influence of vertical strain. Furthermore, it is discovered that the AB DLHS-AlAs/germanene vdWH is capable of undergoing a transition from a semiconductor to a metal state under a vertical strain of 16%. The results of optical properties reveal that all vdWHs exhibit enhanced light absorption across the ultraviolet to visible light range, compared to their individual components. The application of vertical strain can result in the weakening or enhancement of ultraviolet light absorption coefficients in different regions of all vdWHs. It is also noteworthy that the optical adsorption in the visible light region for all vdWHs is consistently enhanced and broadened with increasing vertical compression strain. These significant findings collectively demonstrate that the DLHS-AlAs/germanene vdWHs exhibit superior photoelectric properties compared to their individual components. Furthermore, the vertical compression strain has been observed to significantly enhance and improve the optoelectronic properties of vdWHs, indicating their potential for favourable applications in optoelectronic devices.

CRediT authorship contribution statement

Gang Guo: Writing – review & editing, Writing – original draft, Visualization, Validation, Supervision, Software, Resources, Investigation, Funding acquisition, Formal analysis, Data curation, Conceptualization. **Yongcheng Chen:** Writing – original draft, Visualization, Methodology, Investigation, Data curation. **Lingyun Mao:** Writing – original draft, Visualization, Funding acquisition, Data curation. **Ping Li:** Visualization, Supervision, Software, Resources, Methodology, Investigation, Formal analysis.

Declaration of competing interest

The authors declare that they have no known competing financial interests or personal relationships that could have appeared to influence the work reported in this paper.

Acknowledgments

This work is supported by Scientific Research Fund of Hunan Provincial Education Department (Grant No. 20C0571), the College Students' Innovation and Entrepreneurship Training Program of Hunan Province (S202411528135).

Supplementary materials

Supplementary material associated with this article can be found, in the online version, at doi:10.1016/j.surfin.2024.105413.

Data availability

Data will be made available on request.

References

[1] K.S. Novoselov, A.K. Geim, S.V. Morozov, D. Jiang, Y. Zhang, S.V. Dubonos, I. V. Grigorieva, A.A. Firsov, Electric field effect in atomically thin carbon films, Science (1979) 306 (2004) 666–669.

[2] J.C. Meyer, A.K. Geim, M.I. Katsnelson, et al., The structure of suspended graphene sheets, Nature 446 (7131) (2007) 60–63.

[3] J.W. Burress, S. Gadipelli, J. Ford, et al., Graphene oxide framework materials: theoretical predictions and experimental results, Angewandte Chemie Int. Ed. 49 (47) (2010) 8902–8904.

[4] S. Adam, E.H. Hwang, V.M. Galitski, et al., A self-consistent theory for graphene transport, Proc. Natl. Acad. Sci. 104 (47) (2007) 18392–18397.

[5] Y. Zhang, Y.W. Tan, S.H.L. tormer, et al., Experimental observation of the quantum Hall effect and Berry's phase in graphene, Nature 438 (7065) (2005) 201–204.

[6] A.F. Carvalho, B. Kulyk, A.J.S. Fernandes, et al., A review on the applications of graphene in mechanical transduction, Adv. Mater. 34 (8) (2022) 2101326.

[7] P. Wu, Q. Shao, Y. Hu, et al., Direct electrochemistry of glucose oxidase assembled on graphene and application to glucose detection, Electrochim. Acta 55 (28) (2010) 8606–8614.

[8] A. Kara, H. Enriquez, A.P. Seitsonen, L.L.Y. Voon, S. Vizzini, B. Aufray, H. Oughaddou, A review on silicene-new candidate for electronics, Surf. Sci. Rep. 67 (2012) 1–18.

[9] S. Cahangirov, M. Topsakal, E. Aktürk, H.S. ahin, S. Ciraci, Two- and one dimensional honeycomb structures of silicon and germanium, Phys. Rev. Lett. 102 (2009) 236804.

[10] Z. Li, J. Han, S. Cao, et al., Physical properties of monolayer Mn $(BiTeS)_2$ and its applications in sub–3 nm spintronic devices, Phys. Rev. B 108 (18) (2023) 184413.

[11] L. Li, S. Lu, J. Pan, et al., Buckled germanene formation on Pt (111), Adv. Mater. 26 (28) (2014) 4820–4824.

[12] M.E. Dávila, L. Xian, S. Cahangirov, et al., Germanene: a novel two-dimensional germanium allotrope akin to graphene and silicene, New J. Phys. 16 (9) (2014) 095002.

[13] M. Derivaz, D. Dentel, R. Stephan, et al., Continuous germanene layer on Al (111), Nano Lett. 15 (4) (2015) 2510–2516.

[14] C.H. Lin, A. Huang, W.W. Pai, et al., Single-layer dual germanene phases on Ag (111), Phys. Rev. Mater. 2 (2) (2018) 024003.

[15] S. Balendhran, S. Walia, H. Nili, et al., Elemental analogues of graphene: silicene, germanene, stanene, and phosphorene, Small. 11 (6) (2015) 640–652.

[16] R. Singh, Spin-orbit coupling in graphene, silicene and germanene: dependence on the configuration of full hydrogenation and fluorination, Bull. Mater. Sci. 41 (6) (2018) 1–7.

[17] L. Seixas, J.E. Padilha, A. Fazzio, Quantum spin Hall effect on germanene nanorod embedded in completely hydrogenated germanene, Phys. Rev. B 89 (19) (2014) 195403.

[18] P. Snehha, V. Nagarajan, R. Chandiramouli, Germanene nanotube electroresistive molecular device for detection of NO_2 and SO_2 gas molecules: a first-principles investigation, J. Comput. Electron. 18 (1) (2019) 308–318.

[19] X. Si, W. She, Q. Xu, et al., First-principles density functional theory study of modified germanene-based electrode materials, Materials (Basel) 15 (1) (2021) 103.

[20] C. Feng, J. Ouyang, Z. Tang, et al., Germanene-based theranostic materials for surgical adjuvant treatment: inhibiting tumor recurrence and wound infection, Matter. 3 (1) (2020) 127–144.

[21] Y. Jing, X. Zhang, D. Wu, et al., High carrier mobility and pronounced light absorption in methyl-terminated germanene: insights from first-principles computations, J. Phys. Chem. Lett. 6 (21) (2015) 4252–4258.

[22] Y.F. Zhu, Q.Q. Dai, M. Zhao, et al., Physicochemical insight into gap openings in graphene, Sci. Rep. 3 (1) (2013) 1–8.

[23] F. Teng, K. Hu, W. Ouyang, et al., Photoelectric detectors based on inorganic p-type semiconductor materials, Adv. Mater. 30 (35) (2018) 1706262.

[24] X.K. Chen, X.Y. Hu, P. Jia, et al., Tunable anisotropic thermal transport in porous carbon foams: the role of phonon coupling, Int. J. Mech. Sci. 206 (2021) 106576.

[25] X.K. Chen, E.M. Zhang, D. Wu, et al., Strain-induced medium-temperature thermoelectric performance of Cu_4TiSe_4: the role of four-phonon scattering, Phys. Rev. Appl. 19 (4) (2023) 044052.

[26] G. Guo, Y.M. Shi, et al., First-principles study on the electronic and magnetic properties of P edge doped armchair germanium selenide nanoribbon, Comput. Mater. Sci. 172 (2020) 109348.

[27] G. Guo, G.C. Guo, First-principles study on the electronic, magnetic and optical properties of the novel squared SN_2 monolayer with 3d transition metal doping and point vacancy, Res. Phys. 57 (2024) 107396.

[28] Q. Liu, J.J. Li, D. Wu, et al., Gate-controlled reversible rectifying behavior investigated in a two-dimensional MoS_2 diode, Phys. Rev. B 104 (4) (2021) 045412.

[29] X.D. Huang, Q. Liu, H.Q. Xie, et al., Transport properties of 5-nm tunnel field-effect transistor for high-performance switches decorated with blue phosphorene and transition metals, IEEE Trans. Electron. Dev. 70 (2023) 5462–5468.

[30] M.A. Van Hove, From surface science to nanotechnology, Catal. Today 113 (3–4) (2006) 133–140.

[31] M. Gibertini, M. Koperski, A.F. Morpurgo, et al., Magnetic 2D materials and heterostructures, Nat. Nanotechnol. 14 (5) (2019) 408–419.

[32] D. Xu, J. Ru, B. Cai, et al., Theoretical design of a multifunctional two-dimensional Hf $GeTe_4$-based optoelectronic device utilizing the anisotropic photogalvanic effect, Phys. Rev. Appl. 20 (5) (2023) 054025.

[33] Y.L. Mao, C.S. Xu, J.M. Yuan, et al., A two-dimensional GeSe/SnSe heterostructure for high performance thin-film solar cells, J. Mater. Chem. A 7 (18) (2019) 11265–11271.

[34] Y. Qin, L. Zhao, J. Xie, et al., Theoretical approach to boosting NH_3-sensing based on GeSe/SnS vdW heterostructure with strain modulation, Appl. Surf. Sci. 600 (2022) 154080.

[35] K.L. Seyler, P. Rivera, H. Yu, et al., Signatures of moiré-trapped valley excitons in $MoSe_2/WSe_2$ heterobilayers, Nature 567 (7746) (2019) 66–70.

[36] J.C. in, E.C. Regan, A. Yan, et al., Observation of moiré excitons in WSe_2/WS_2 heterostructure superlattices, Nature 567 (7746) (2019) 76–80.

[37] Q. Luo, S. Yin, X. Sun, et al., Interlayer coupling and external electric field controllable electronic structures and Schottky contact of HfSeX (X= S, Se)/ graphene van der Waals heterostructures, Diam. Relat. Mater. 128 (2022) 109223.

[38] K. Roy, M. Padmanabhan, S. Goswami, et al., Graphene-MoS_2 hybrid structures for multifunctional photoresponsive memory devices, Nat. Nanotechnol. 8 (11) (2013) 826–830.

[39] T. Georgiou, R. Jalil, B.D. Belle, et al., Vertical field-effect transistor based on graphene-WS_2 heterostructures for flexible and transparent electronics, Nat. Nanotechnol. 8 (2) (2013) 100–103.

[40] J.Y. Tan, A. Avsar, J. Balakrishnan, et al., Electronic transport in graphene-based heterostructures, Appl. Phys. Lett. 104 (18) (2014) 183504.

[41] Q. Feng, B. Huang, X. Li, Graphene-based heterostructure composite sensing materials for detection of nitrogen-containing harmful gases, Adv. Funct. Mater. 31 (41) (2021) 2104058.

[42] J. Zhang, B. Zhao, Y. Yao, Quantum anomalous Hall effect in graphene-based heterostructure, Sci. Rep. 5 (1) (2015) 1–8.

[43] M. Zeng, L. Shen, M. Yang, et al., Charge and spin transport in graphene-based heterostructure, Appl. Phys. Lett. 98 (5) (2011) 053101.

[44] X. He, X.Q. Deng, L. Sun, et al., Electronic and optical properties and device applications for antimonene/WS_2 van der Waals heterostructure, Appl. Surf. Sci. 578 (2022) 151844.

[45] S.M. Mozvashi, S.I. Vishkayi, M.B. Tagani, Antimonene/bismuthene vertical van-der waals heterostructure: a computational study, Physica E 118 (2020) 113914.

[46] A. Sengupta, A. Dominguez, T. Frauenheim, Photo-absorption properties of van der Waals heterostructure of monolayer InSe with silicene, germanene and antimonene, Appl. Surf. Sci. 475 (2019) 774–780.

[47] Q. Pang, H. Xin, D. Gao, et al., Strain effect on the electronic and optical properties of Germanene/MoS2 heterobilayer, Mater. Today Commun. 26 (2021) 101845.

[48] K. Zheng, Q. Yang, C.J. Tan, et al., A two-dimensional van der Waals CdS/ germanene heterojunction with promising electronic and optoelectronic properties: DFT+ NEGF investigations, Phys. Chem. Chem. Phys. 19 (28) (2017) 18330–18337.

[49] M.S. Islam, M.R.H. Mojumder, N. Ferdous, et al., Germanene/2D-SiC van der Waals heterobilayer: structural features and tunable electronic properties, Mater. Today Commun. 26 (2021) 101718.

[50] H.Y. Ye, F.F. Hu, H.Y. Tang, et al., Germanene on single-layer ZnSe substrate: novel electronic and optical properties, Phys. Chem. Chem. Phys. 20 (23) (2018) 16067–16076.

[51] M. Faraji, A. Bafekry, M.M. Fadlallah, et al., Two-dimensional XY monolayers (X= Al, Ga, In; Y= N, P, As) with a double layer hexagonal structure: a first-principles perspective, Appl. Surf. Sci. 590 (2022) 152998.

[52] L. Qin, Z.H. Zhang, Z. Jiang, K. Fan, W.H. Zhang, Q.Y. Tang, H.N. Xia, F. Meng, Q. Zhang, Y.S. Fu, et al., Realization of AlSb in the double-layer honeycomb structure: a robust class of two-dimensional material, ACS. Nano (2021).

[53] D. Pan, D.X. Fan, N. Kang, et al., Free-standing two-dimensional single-crystalline InSb nanosheets, Nano Lett. 16 (2) (2016) 834–841.

[54] G. Kresse, D. Joubert, From ultrasoft pseudopotentials to the projector augmented-wave method, Phys. Rev. B 59 (3) (1999) 1758.

[55] G. Kresse, J. Joubert, From ultrasoft pseudopotentials to the projector augmentedwave method, Phys. Rev. B 59 (1999) 1758–1775.

[56] J.P. Perdew, K. Burke, M. Ernzerhof, Generalized gradient approximation made simple, Phys. Rev. Lett. 77 (18) (1996) 3865.

[57] B. Hammer, L.B. Hansen, J.K. Nørskov, Improved adsorption energetics within density-functional theory using revised Perdew-Burke-Ernzerhof functionals, Phys. Rev. B 59 (11) (1999) 7413.

[58] J. Heyd, G.E. Scuseria, M. Ernzerhof, Hybrid functionals based on a screened Coulomb potential, J. Chem. Phys. 118 (18) (2003) 8207–8215.

[59] S. Grimme, J. Antony, S. Ehrlich, H. Krieg, A consistent and accurate ab initio parametrization of density functional dispersion correction (DFT-D) for the 94 elements H-Pu, J. Chem. Phys. 132 (2010) 154104.

[60] S. Baroni, S.D. Gironcoli, A.D. Corso, Phonons and related crystal properties from density-functional perturbation theory, Rev. Mod. Phys. 73 (2001) 516–562.

[61] D.M. Hoat, D.K. Nguyen, R. Ponce-Perez, et al., Opening the germanene monolayer band gap using halogen atoms: an efficient approach studied by first-principles calculations, Appl. Surf. Sci. 551 (2021) 149318.

[62] C. Tan, Q. Yang, R. Meng, et al., An AlAs/germanene heterostructure with tunable electronic and optical properties via external electric field and strain, J. Mater. Chem. C 4 (35) (2016) 8171–8178.

[63] H.F. Lin, H.Y. Liu, W. Wang, et al., Janus Ga_2SeTe/In_2SSe heterostructures: tunable electronic, optical, and photocatalytic properties, Phys. Chem. Chem. Phys. 24 (7) (2022) 4425–4436.

[64] D. Ge, R. Luo, X. Wang, et al., Internal and external electric field tunable electronic structures for photocatalytic water splitting: janus transition-metal chalcogenides/C_3N_4 van der Waals heterojunctions, Appl. Surf. Sci. 566 (2021) 150639.

[65] K.D. Pham, N.N. Hieu, H.V. Phuc, et al., Layered graphene/GaS van der Waals heterostructure: controlling the electronic properties and Schottky barrier by vertical strain, Appl. Phys. Lett. 113 (2018) 171605.

[66] A. Bafekry, C. Stampfl, M. Naseri, et al., Effect of electric field and vertical strain on the electro-optical properties of the $MoSi_2N_4$ bilayer: a first-principles calculation, J. Appl. Phys. 129 (2021) 155103.

[67] N. Zhao, U. Schwingenschlögl, Transition from Schottky to Ohmic contacts in Janus MoSSe/germanene heterostructures, Nanoscale 12 (21) (2020) 11448–11454.